High-field magnetization and magnetic structure of Tb_3Co

2007 J. Phys.: Condens. Matter 19 326213

(http://iopscience.iop.org/0953-8984/19/32/326213)

IOP PUBLISHING JOURNAL OF PHYSICS: CONDENSED MATTER

J. Phys.: Condens. Matter **19** (2007) 326213 (14pp) doi:10.1088/0953-8984/19/32/326213

High-field magnetization and magnetic structure of Tb_3Co

N V Baranov[1,2,5], A F Gubkin[2], A P Vokhmyanin[1], A N Pirogov[1], A Podlesnyak[3], L Keller[4], N V Mushnikov[1] and M I Bartashevich[2]

[1] Institute of Metal Physics, Russian Academy of Science, 620041 Ekaterinburg, Russia
[2] Institute of Physics and Applied Mathemathics, Ural State University, 620083 Ekaterinburg, Russia
[3] Hahn-Meitner-Institut, SF-2, Glienicker Straße 100, Berlin 14109, Germany
[4] Laboratory for Neutron Scattering, ETH Zurich and Paul Scherrer Institut, CH-5232 Villigen PSI, Switzerland

E-mail: nikolai.baranov@usu.ru

Received 11 April 2007, in final form 12 June 2007
Published 16 July 2007
Online at stacks.iop.org/JPhysCM/19/326213

Abstract

The measurements of the magnetization in high steady and pulsed fields together with neutron diffraction measurements on a powder sample and on a single crystal have been performed to study the magnetic state of the Tb_3Co compound. It has been shown that the modulated antiferromagnetic structure which exists in Tb_3Co below $T_N = 82$ K transforms to the incommensurate magnetic structure with a strong ferromagnetic component along the *c*-axis with further cooling below the critical temperature $T_t \approx 72$ K. The phase transition from the high-temperature to the low-temperature magnetic state at T_t is of first order. The incommensurability of the low-temperature magnetic structure of Tb_3Co is attributed to the non-Kramers character of the Tb^{3+} ion in combination with competition between the indirect exchange interaction and the low-symmetry crystal electric field.

(Some figures in this article are in colour only in the electronic version)

1. Introduction

The family of objects exhibiting magnetic structures incommensurate with the crystal lattice has broadened substantially in last two decades. This is because new classes of rare-earth (R) intermetallic compounds (binary and ternary) have been synthesized and studied and new generations of neutron scattering techniques have been developed during this period. New instruments with enhanced resolution, position-sensitive detectors with large covered angle

[5] Address for correspondence: Ural State University, Lenin avenue 51, 620083 Ekaterinburg, Russia.

range and improved sample environment conditions allow the detection of weak reflections which could not be identified before. Some binary and pseudo-binary rare-earth compounds with magnetic as well as non-magnetic partners, which were known for a long time and thought to exhibit simple magnetic structures, have revealed a much more complex magnetic behaviour [1–5]. Numerous rare-earth intermetallic systems having a strong magnetocrystalline anisotropy were observed to be incommensurate not only just below magnetic ordering temperatures but at very low temperatures as well. This often occurs when the R ion is a non-Kramers one. In this case the incommensurate modulated structures can be stable down to 0 K [1]. The presence of incommensurate magnetic structures in rare-earth intermetallics is associated with competition between different interactions (mainly between the long-range exchange interaction of RKKY (Ruderman–Kittel–Kasuya–Yosida) type and the crystalline electric field) and thermal energy. These compounds may exhibit field-induced phase transitions and very complex magnetic phase diagrams. A rich variety of field-induced phase transitions and noncollinear antiferromagnetic (AF) or ferromagnetic (FM) structures have been observed in some R_3M compounds (M = Co, Ni, Rh) [6–13]. The R_3M compounds have the largest content of the rare-earth metal among the binary R–M compounds and crystallize in the low-symmetry orthorhombic crystal structure of the Fe_3C type (space group $Pnma$) [14]. Rare-earth atoms occupy two nonequivalent positions, 4c and 8d. The d-transition metal atoms are located at the 4c site within trigonal prisms formed by R ions. The presence of two incommensurate magnetic structures was recently revealed in Ho_3Co by neutron diffraction measurements performed on powder as well as on single-crystalline samples [15]: AF_{II} in the temperature interval from $T_t \approx 8$ K up to the Néel temperature $T_N = 22$ K and AF_I below 8 K. Moreover, in the AF_I structure, the presence of a small ferromagnetic component was revealed along the a-axis of the Ho_3Co single crystal [13]. These magnetic structures were suggested to arise from the non-Kramers character of Ho^{3+} ions and the competition between the RKKY exchange interaction and crystal-field effects.

The present paper focuses on the magnetic structure and peculiarities of the magnetic behaviour of the Tb_3Co compound. According to the previous neutron diffraction study [7, 16] this compound undergoes a phase transition from the paramagnetic state to the AF state with modulated structure with decreasing temperature below $T_N = 82$ K. Further cooling below the critical temperature $T_t = 72$ K is suggested to lead to a complex noncoplanar magnetic structure with FM alignment of projections of Tb magnetic moments onto the c-axis and with AF ordering of the projections onto the a- and b-axes. Below T_t, the magnetic structure of Tb_3Co was suggested to be commensurate with the crystal lattice [7, 16]. The Co atoms in Tb_3Co as in other R_3Co do not possess their own magnetic moment. However, the itinerant 3d-electron subsystem of Co substantially affects the physical properties (electrical resistivity, specific heat and magnetic characteristics) of these compounds [17]. At low temperatures, the magnetization process along the c-axis of a Tb_3Co single crystal was found to be typical for ferromagnetic compounds with narrow domain walls [18]. The high remnant magnetization together with the large coercive field observed along the c-axis of a Tb_3Co single crystal at low temperatures results in the highest energy product (up to 140 MG Oe at $T \sim 4$ K [9]) within the rare-earth–3d-metal intermetallics. The phase transitions along the a- and b-axes induced by an applied magnetic field are observed to be accompanied in Tb_3Co by significant changes in the electrical resistivity [9]. However, a large positive magnetoresistance effect observed at the field-induced AF–FM transition along the a-axis [9] can hardly be explained by simple spin-flip processes within the model of the commensurate magnetic structure, bearing in mind that the AF–FM transitions under application of a magnetic field are usually accompanied by negative magnetoresistance due to superzone effects (see [19], for instance). Therefore, one can suggest the presence of more complicated magnetic structures in Tb_3Co at low temperatures.

In this work, the measurements of the magnetic susceptibility and magnetization in steady and pulsed magnetic fields as well as the neutron diffraction in a wide temperature range on powder and single-crystalline samples were used in order to examine the magnetic state and to achieve a better understanding of unusual properties of the Tb_3Co compound as well as all the R_3M series.

2. Experimental details

The Tb_3Co compound was obtained by arc melting in a helium atmosphere using Tb and Co of 99.9 and 99.99% purity, respectively. Single crystals were grown by the Bridgman method in a resistance furnace. The phase purity of single crystals was checked by a metallographic method. The content of foreign phases was estimated to be less than 3%. The magnetization measurements were made on the sample of about $2 \times 2 \times 2$ mm^3 in size by a home-made vibrating sample magnetometer in magnetic fields up to 70 kOe and by an extraction-type magnetometer in fields up to 180 kOe applied along the main crystallographic directions. The dc magnetic susceptibility was measured using a SQUID magnetometer (Quantum Design, USA). High magnetic fields up to 420 kOe were produced using a wire-wound pulsed magnet with a duration time of about 20 ms. The magnetization in pulsed fields was measured by an induction method with a set of compensated pickup coils at temperatures from 1.5 to 50 K. Magnetization measurements in high steady and pulsed fields were performed at the Institute for Solid State Physics, University of Tokyo.

Neutron powder diffraction (NPD) measurements were performed on a cold neutron powder diffractometer (DMC) at the spallation neutron source SINQ at the Paul Scherrer Institute, Switzerland, using the wavelengths $\lambda = 3.88$ and 2.56 Å. For the refinement of the magnetic structure the program FullProf [20] was used. The single-crystal investigation was carried out using the double-axis diffractometer E4 installed at the BENSC Hahn-Meitner-Institut in Berlin, with the incident neutron wavelength 2.438 Å. The measurements were made on a parallelepiped sample of size $1 \times 1 \times 5$ mm^3 with long side parallel to the *c*-axis oriented vertically.

3. Results and discussion

3.1. Magnetic susceptibility and magnetization measurements

As follows from figure 1, the temperature dependences of the magnetization measured at a low field (50 Oe) along main crystallographic directions of the Tb_3Co single crystal show distinct anomalies at $T_N = 82$ K and $T_t = 72$ K. These anomalies are more pronounced when the field is applied along the *c*-axis. A drastic increase of the magnetization along the *c*-axis with increasing temperature above 30 K is associated with the thermal activation of the motion of narrow domain walls, which were frozen at low temperatures. An analogous behaviour of the $M(T)$ dependence was observed for other high-anisotropic systems, such as for Dy_3Al_2 [21] and $Tb_{0.5}Y_{0.5}Ni$ [22]. The presence of a significant anisotropy in Tb_3Co, which is revealed by low-field magnetization measurements below 130 K, is supported by the magnetic susceptibility data obtained in the paramagnetic region. The reciprocal susceptibility is strongly anisotropic (see figure 2) and demonstrates nearly linear temperature dependence above 150 K for all principal crystallographic directions. The estimation of the effective magnetic moment gives values of $\mu_{eff} = 10.2$–$10.6\ \mu_B$ depending on the direction of measurements (see table 1). The anisotropy of μ_{eff} may be attributed to low measuring temperatures in comparison with the total splitting of the ground-state $^7F_6$ multiplet of Tb^{3+} ion in the crystalline electric field.

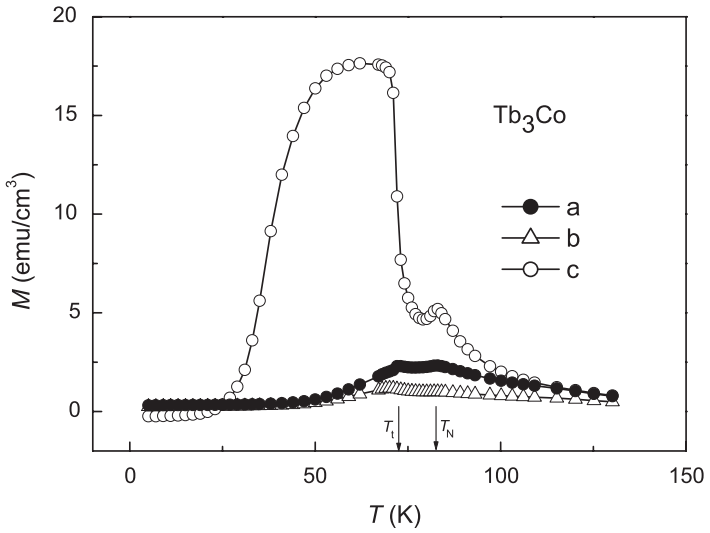

Figure 1. Temperature dependence of the magnetization measured at $H = 50$ Oe along principal crystallographic directions of a Tb_3Co single crystal.

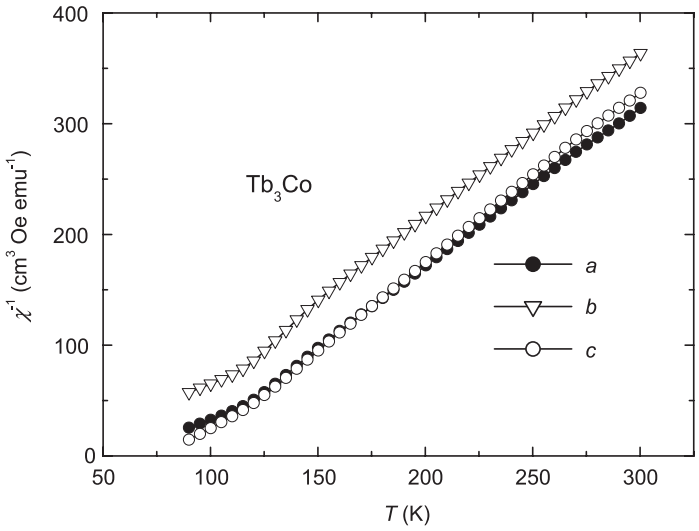

Figure 2. Temperature dependence of the reciprocal susceptibility measured along main crystallographic directions of Tb_3Co.

The strong influence of the crystal field in Tb_3Co is explicitly evidenced by the presence of a large anisotropy of the paramagnetic Curie temperatures, Θ_p, which are estimated to be about of 86, 55 and 91 K for *a*-, *b*- and *c*-axes respectively. These data indicate that the *c*-axis should be an easy magnetization direction while the *b*-axis is a hard direction. Note that for the isostructural Er_3Co compound the minimal value of Θ_p was observed along the *a*-axis, and the maximal Θ_p was obtained for the *b*-axis [23]. The difference in the easy axis directions in both compounds may be attributed to the different sign of the Steven's factor α_J for Tb^{3+} and Er^{3+} ions [24]. Unfortunately, one cannot unambiguously determine the crystal-field parameters for Tb_3Co, due to the low symmetry of the two nonequivalent crystallographic positions of R ions in the Fe_3C-type lattice. The value of μ_{eff} per Tb ion for Tb_3Co obtained from $1/\chi$ versus T dependences at temperatures 150–300 K surpasses $\mu_{eff} = 9.72\ \mu_B$ for the free Tb^{3+} ion. The additional contribution to the effective magnetic moment $\Delta\mu_{eff} \approx 0.5$–$0.9\ \mu_B$ per Tb ion in Tb_3Co may be attributed to spin fluctuations induced by the f–d exchange interaction in the

Table 1. Magnetic characteristics of Tb_3Co: paramagnetic Curie temperature Θ_p, effective magnetic moment per Tb ion μ_{eff}, projections of the Tb magnetic moment onto ith axis for 4c and 8d sites in the Fe_3C lattice according to neutron diffraction measurements [7], average value of the projection of the Tb magnetic moment ($\bar{M}_i$ (neutr)) onto ith axis of Tb_3Co according to [7], and average value of the magnetization per Tb ion ($\bar{M}_i$ (magn)) obtained by extrapolation of $M(H)$ curves which are measured along the ith axis in high magnetic fields.

	$\Theta_p(K)$ Present work	μ_{eff} (μ_B/Tb) Present work	M_i (μ_B/Tb) 4c (neutr) Reference [7]	M_i (μ_B/Tb) 8d (neutr) Reference [7]	$\bar{M}_i$ (neutr) (μ_B/Tb) (neutr) Reference [7]	$\bar{M}_i$ (magn) (μ_B/Tb) (bulk magn.) Present work
a	86	10.6	3.9 ± 0.3	2.7 ± 0.3	3.1 ± 0.3	7.3
b	55	10.5	0	3.9 ± 0.3	2.6 ± 0.3	6.3
c	91	10.2	7.9 ± 0.5	7.4 ± 0.5	7.6 ± 0.3	7.6

itinerant d-electron subsystem [17]. Unlike Tb_3Co, the magnetic susceptibility measurements of Er_3Co single crystals have shown [23] that the effective moment calculated per Er ion is close to μ_{eff} for the free Er^{3+} ion, i.e. $\Delta\mu_{eff} \approx 0$. Bearing in mind a higher spin value for Tb ($S = 3$) in comparison with Er ($S = 3/2$) the difference in $\Delta\mu_{eff}$ values for Tb_3Co and Er_3Co may be considered as evidence of the induced character of this extra contribution to the effective moment.

It should be noted that for the R–Co intermetallics the following two opposite tendencies are known: the magnetic moment of Co ions decreases with increasing R content, while the energy of the f–d exchange interaction increases [25, 26]. The fact that the 3d M ions in the Fe_3C-type lattice are surrounded by rare-earth ions together with the large distance between M ions (∼4 Å) results in the significant 5d(R)–d(M) hybridization [27] and implies a strong influence of the 4f electrons of M ions on the d electrons of the transition metal, despite the M ions not possessing ordered magnetic moments in R_3M. The exchange field that arises from localized 4f electrons of the R ion should lead to polarization of the 5d electrons on the same R ion and then spin fluctuations are induced in the d-electron subsystem of M ions through the R 5d–Md hybridization. In this case the local amplitude of spin fluctuations and, consequently, their effect upon different physical properties are expected to depend on the spin value of the R ion. The significant influence of the spin fluctuation contribution may cause the excess of the effective magnetic moment, which was revealed for other R_3M compounds (M = Ni, Rh). Thus, within the R_3Ni series with heavy rare-earth elements the value of $\Delta\mu_{eff}$ per R ion was found to decrease gradually from ∼1.1 μ_B down to 0.47 μ_B with increasing atomic number from Gd to Er, i.e. with decreasing spin value of the R ion [28]. The reduction of $\Delta\mu_{eff}$ from 0.55 μ_B to 0.02 μ_B was also revealed for the R_3Rh family when going from R = Gd to R = Er (see [29] and references therein). The influence of spin fluctuations in R_3M is also supported by low-temperature specific heat data for Gd_3M and Y_3M (M = Co, Ni, Rh) compounds. The coefficient of the electronic specific heat for Gd_3M was observed to be about one order higher (γ = 100–170 mJ $mol^{-1}K^{-2}$) than that obtained for isostructural Y_3M compounds (γ = 11–15 mJ mol^{-1} K^{-2}) [30, 31]. Such a great difference in γ for Gd_3M and Y_3M compounds is attributed to huge contribution due to spin fluctuations induced by the 4f electrons of Gd in the d electron subsystem of the M transition metal via f–d exchange bearing in mind the high spin value of the 4f electron shell ($S = 7/2$) of Gd ions and the absence of the self-magnetic moment on Y ions in Y_3M [17, 30, 31].

The results of the magnetization measurements on a Tb_3Co single crystal in high steady magnetic fields (up to 180 kOe) and in high pulse fields (up to 420 kOe) are presented in figures 3 and 4. In general, the magnetization data are in agreement with the magnetic structure

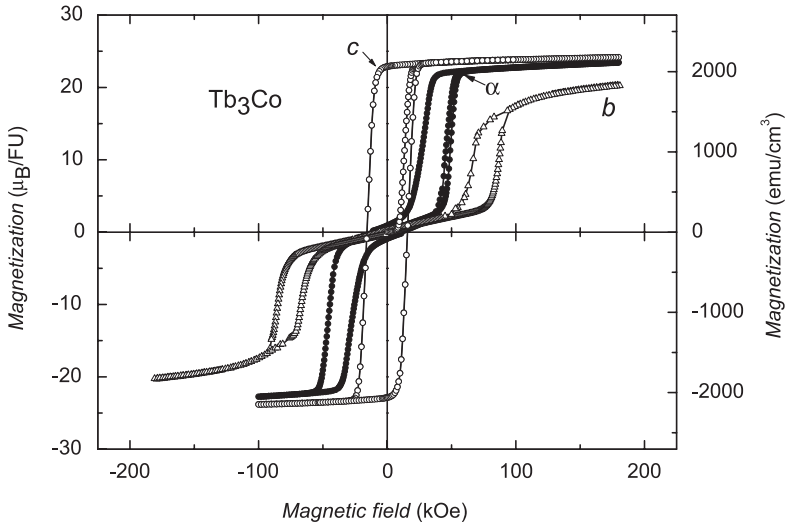

Figure 3. Field dependences of the magnetization measured along main axes of a Tb_3Co single-crystalline sample at $T = 4.2$ K in steady fields up to 180 kOe.

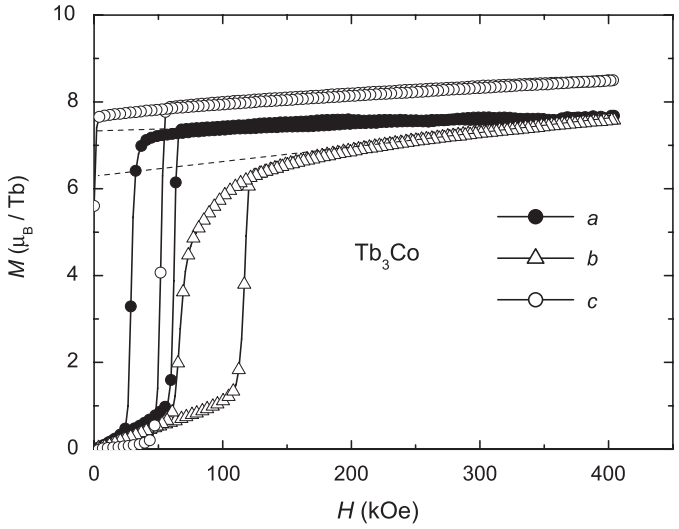

Figure 4. Field dependences of the magnetization per Tb ion measured at $T = 4.2$ K along the main axes of Tb_3Co in pulsed fields up to 420 kOe.

suggested in [16]. The magnetization process in the magnetic field applied along the easy *c*-axis seems to be typical for high-anisotropic ferromagnets with narrow domain walls and shows a large magnetic after-effect which is associated with the thermal activation of the domain wall displacement. Such a mechanism results in a substantial decrease of the coercive field, H_c, with increasing temperature. The H_c value reduces from ∼16 kOe at 4.2 K down to ∼100 Oe above 30 K. At low temperatures, the magnetic moment per Tb ion in Tb_3Co does not reach its theoretical value $gJ\mu_B = 9\ \mu_B$ even when a field up to 420 kOe is applied along the easy *c*-axis (figure 4). Pulse-field experiments revealed the increased critical transition fields and an enhanced hysteresis in comparison with measurements in quasi-static fields. Thus,

from pulse-field measurements at 4.2 K, the $H^a_{\rm crit}$ and $H^b_{\rm crit}$ values along the a- and b-axes were obtained to be about 59 and 110 kOe, while under application of quasi-static fields these values were estimated to be 45 and 81 kOe, respectively. All these observations are indicative of the presence of a very high magnetocrystalline anisotropy caused by crystal-field effects. The step-like increase of the magnetization along the a- and b-axes at critical fields may be associated with the first-order phase transitions occurring via spin-flip processes of the Tb magnetic moments $M_{\rm Tb}$ from the structure having an AF alignment of the projections of the Tb magnetic moments along the a-axis (M_a) and the b-axis (M_b) at $H = 0$ to the field-induced non-collinear structures with the ferromagnetic component along the field directions. When extrapolating the magnetization from the high-field region above the critical fields to $H \to 0$ the M_a, M_b and $M_{\rm c}$ result in being 7.3, 6.3 and 7.6 $\mu_{\rm B}$, respectively. Here we taken into account that the magnetization increases near linearly within accuracy of the pulse-field measurements ($\sim$4%) with increasing field above 30 kOe along the c-axis, above 100 kOe along the a-axis and above 250 kOe along the b-axis. As follows from the table 1, the value of the projection onto the c-axis, $M_{\rm c} = 7.6\ \mu_{\rm B}$, obtained from bulk magnetization measurements agrees well with that derived from neutron diffraction measurements. However, for other axes such a coincidence is not observed. A simple spin-flip process suggests a change of the magnetic moment direction along the local easy axis under application of a magnetic field without the change of the angle between the local easy axis and field direction. In this case, for a field-induced non-collinear structure one can estimate the value of the magnetic moment of the Tb ion since $M_{\rm Tb}$ should be equal to $[(M_a)^2 + (M_b)^2 + (M_{\rm c})^2]^{1/2}$. A similar magnetization process, which occurs by switching of spins along their local easy axes, takes place in Dy_3Co [12]. However, an estimation of the Tb magnetic moment in Tb_3Co, using the M_a, M_b and $M_{\rm c}$ values taken from figure 4, gives $M_{\rm Tb} \approx 12.3\ \mu_{\rm B}$, which significantly exceeds the value 9 $\mu_{\rm B}$ for the Tb^{3+} free ion. This consideration brings us to the conclusion that the magnetization process in Tb_3Co along the a- and c axes cannot be described by a simple spin-flip picture and that the magnetic structure of this compound is more complicated than that proposed earlier [7, 16].

3.2. Neutron diffraction

In order to study the temperature evolution of the magnetic structure of Tb_3Co we have measured NPD patterns in the temperature range from 1.5 to 150 K. The NPD measurements in the paramagnetic state at $T = 150$ K (figure 5) confirmed the correct phase formation and showed close agreement of structural parameters with previously reported data [32]. The best agreement between the experimental and calculated data with the Bragg R factor $\sim$6% was obtained for an orthorhombic unit cell with the following parameters: $a = (6.978 \pm 0.001)$ Å, $b = (9.397 \pm 0.001)$ Å, $c = (6.272 \pm 0.001)$ Å. For the refinement of the crystal structure, we have taken into account the presence of a small amount ($\sim$1%) of pure Tb metal in our sample as a foreign phase. Figures 6 and 7 display the neutron diffraction data obtained in the magnetically ordered state. Note that the larger neutron wavelength was used in this case in order to achieve a better resolution in the low-2Θ region. The NPD pattern corresponding to the paramagnetic state ($T = 200$ K) is shown in figure 6(a) for comparison as well. The neutron diffraction pattern taken at $T = 78$ K, i.e. in between $T_{\rm t}$ and $T_{\rm N}$, exhibits a set of additional reflections relative to those observed above $T_{\rm N}$ (figure 6(b)). The most prominent magnetic peak was observed in a low-angle region. As follows from figure 6(c), a peak with extremely high intensity (by about two orders of magnitude higher other magnetic reflections) appears around $2\Theta = 3.5°$, which is indicative of the formation of a magnetic structure incommensurate with the crystallographic unit cell. The majority of magnetic peaks observed at $T = 78$ K can be indexed with a propagation vector $\mathbf{k} = (\mu, 0, 0)$, $\mu \approx 0.155$. However, some additional

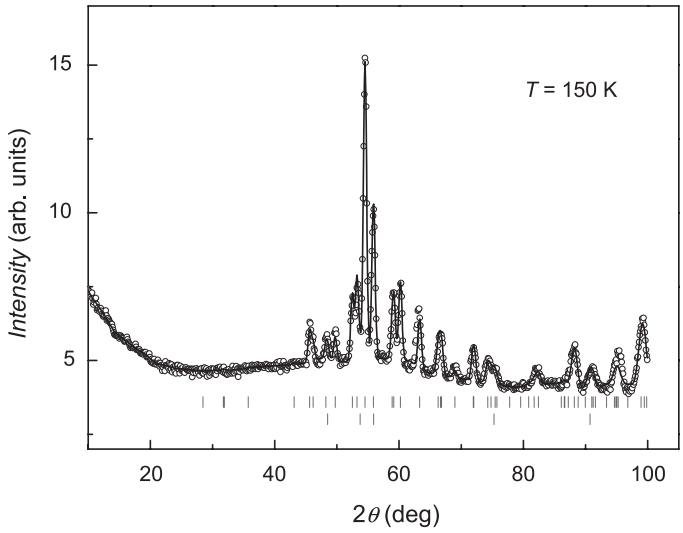

Figure 5. Powder neutron diffraction pattern for Tb_3Co recorded at the neutron wavelength $\lambda = 2.56$ Å in the paramagnetic state at 150 K. The full line through the symbols represents the best fit. The positions of the structural Bragg peaks are marked at the bottom for the Tb_3Co compound (upper row) as well as for the hcp Tb metal as for a foreign phase (lower row).

magnetic reflections were detected, which cannot be indexed with $\mathbf{k} = (\mu, 0, 0)$ (for instance, one is shown in the inset in figure 6(b)). Further lowering the temperature down to $T_t \approx 72$ K results in an appearance of a set of new reflections (see figure 7(a)), whereas the intensities of the reflections with $\mathbf{k} = (\mu, 0, 0)$ vanish. The NPD pattern measured in the vicinity of the phase transition from the high-temperature AF phase to the low-temperature FM phase may result from the superposition of two magnetic structures, indicating thus a first-order transition. It turned out that the magnetic peaks observed below T_t cannot be indexed with $\mathbf{k} = (0, 0, 0)$ only, as was proposed in [7] and [16]. In addition to the $\mathbf{k} = (0, 0, 0)$ set of magnetic reflections, another group can be indexed with the propagation vector $\mathbf{k} = (\beta, \beta, 0)$, $\beta \approx 0.3$ (see figure 7(b)). Therefore, we suggest that the magnetic structure of Tb_3Co below T_t is incommensurate as well. It should also be mentioned that a small-intensity smeared reflection is observed around $2\Theta \sim 4°$–$6°$ in the neutron diffraction pattern measured at 1.5 K (figure 7(b)), i.e. in the same angle interval in which the huge $(000)^+$ satellite was found at temperatures between T_t and T_N. Some traces of the high-temperature AF phase apparently remain within the low-temperature FM phase down to very low temperatures.

In order to check the suggestion about the presence of an incommensurate structure with the ferromagnetic component along the c-axis at $T < T_t$ and to determine the β value more definitely we have performed single-crystal neutron diffraction measurements. Figure 8 shows the scattered neutron intensity along the $[h00]$ direction at 75 and 1.5 K. The neutron diffraction pattern for $T = 75$ K exhibits additional satellites around (200) reflections which were not observed at $T = 1.5$ K. These data, together with the huge satellite peak $(000)^+$ which was observed within the temperature range 65 K $< T <$ 82 K, support our results obtained on powder samples and may be explained by the presence of the incommensurate magnetic structure with the propagation vector $\mathbf{k} = (0.155, 0, 0)$. The new magnetic reflections which are indicative of the incommensurability of the non-collinear ferromagnetic structure below T_t were revealed by $[hh0]$ scans which are shown in figure 9. The neutron diffraction pattern measured at 1.5 K along the $[hh0]$ direction in the $\boldsymbol{a}^*$–$\boldsymbol{b}^*$ reciprocal plane shows the satellite

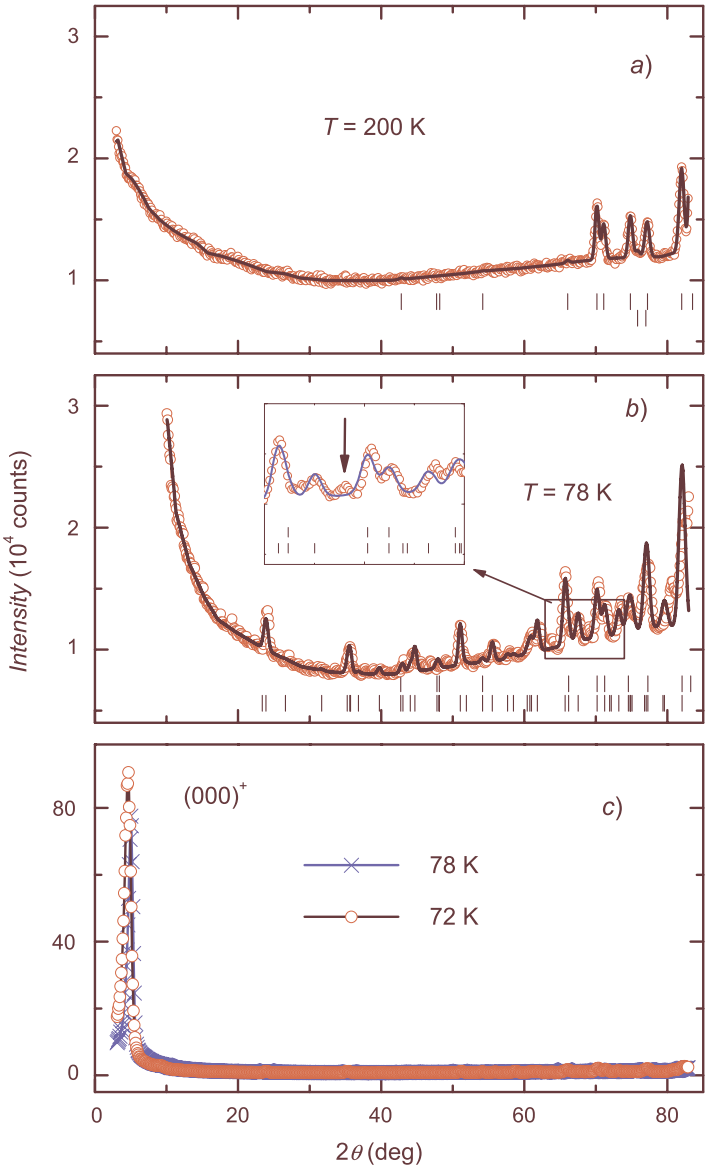

Figure 6. Neutron powder diffraction patterns measured at $\lambda = 3.88$ Å at various temperatures. The full line through the symbols represents the best fit. (a) $T = 200$ K, $3° \leqslant 2\Theta \leqslant 83°$. The upper row of reflection markers refers to the nuclear Bragg peaks for Tb_3Co and the lower row to the impurity of Tb, respectively. (b) $T = 78$ K, $10° \leqslant 2\Theta \leqslant 83°$. The upper row of markers refers to the nuclear Bragg peaks for Tb_3Co and the lower row to magnetic peaks described by the wavevector $\mathbf{k} = (0.155, 0, 0)$. The inset shows a part of the NPD pattern in detail. The arrow indicates the reflection which cannot be described by $\mathbf{k} = (0.155, 0, 0)$. (c) $T = 78$ K (crosses), $T = 72$ K (open circles), $3° \leqslant 2\Theta \leqslant 83°$.

reflections in the vicinity of the (110) reflection, while such satellites are not observed above T_t. Therefore, we may conclude that two wavevectors, $\mathbf{k} = (0, 0, 0)$ and $\mathbf{k} = (\beta, \beta, 0)$ with $\beta \approx 0.32$, have to be used to describe the magnetic structure of Tb_3Co at the $T < T_t$.

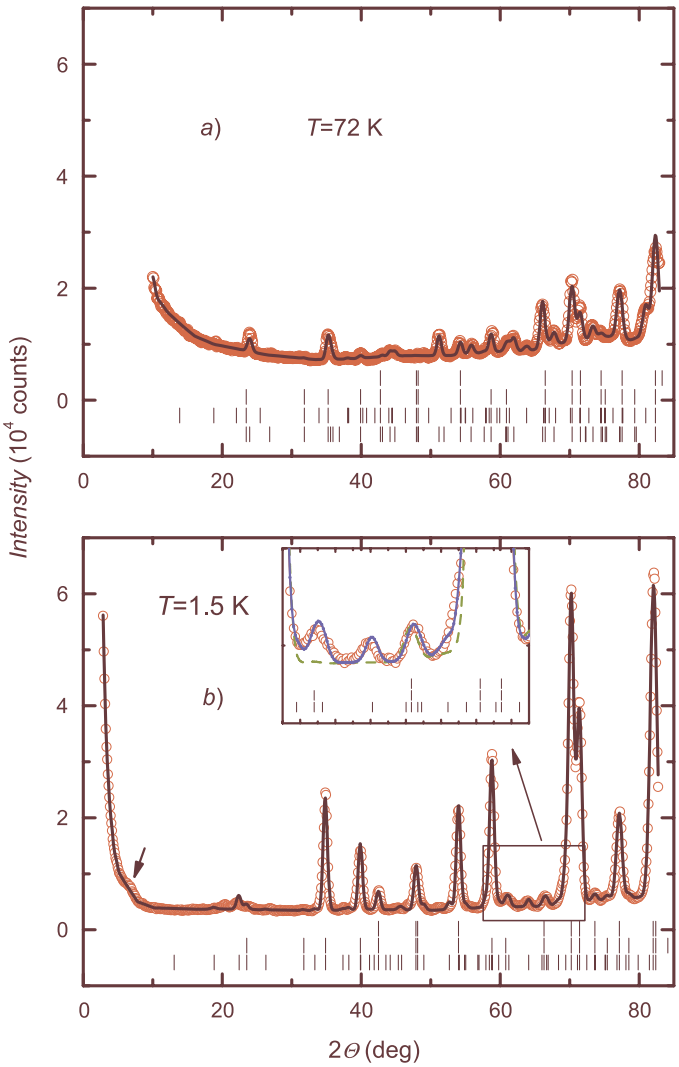

Figure 7. (a) The NPD pattern measured at $\lambda = 3.88$ Å at $T = 72$ K. The full line through the symbols represents the best fit. The sets of vertical marks correspond to the Bragg positions for the nuclear (upper row) and incommensurate phases described by wavevectors $\mathbf{k} = (0, 0, 0)$, $\mathbf{k} = (0.3, 0.3, 0)$ and $\mathbf{k} = (0.155, 0, 0)$, respectively. (b) The NPD pattern measured at $\lambda = 3.88$ Å and at $T = 1.5$ K. The sets of vertical marks correspond to the Bragg positions for the nuclear (upper row) and incommensurate phases described by wavevectors $\mathbf{k} = (0, 0, 0)$ and $\mathbf{k} = (0.3, 0.3, 0)$ respectively. The arrow in the small-angle region indicates the trace intensity associated with high-temperature incommensurate phase. The inset shows a part of the NPD pattern in detail. The dashed line corresponds to the pattern calculated with $\mathbf{k} = (0, 0, 0)$, while the solid line is obtained with $\mathbf{k} = (0.3, 0.3, 0)$.

The change of the magnetic states of Tb_3Co from the incommensurate magnetic structure with the F component along the *c*-axis to the incommensurate AF structure at the critical temperature T_t and finally to the paramagnetic state with further increasing temperature above T_N is clearly seen in the temperature dependences of the integrated intensities of the $(110)^-$ and $(000)^+$ satellites and (110) peak presented in figure 10. The integrated intensities of both the

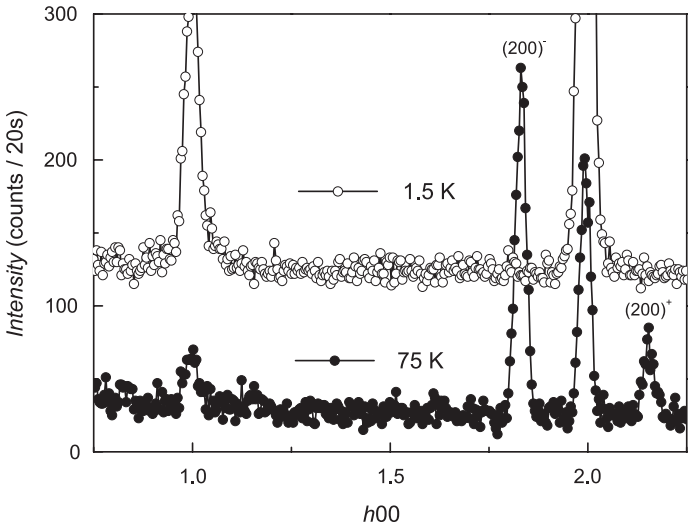

Figure 8. Variation of the intensity of neutron scattering along the [h00] direction in the $\boldsymbol{a}^*$–$\boldsymbol{b}^*$ plane of the reciprocal lattice of a Tb_3Co single crystal at $T = 75$ K (full circles) and $T = 1.5$ K (open circles). The patterns are shifted from each other.

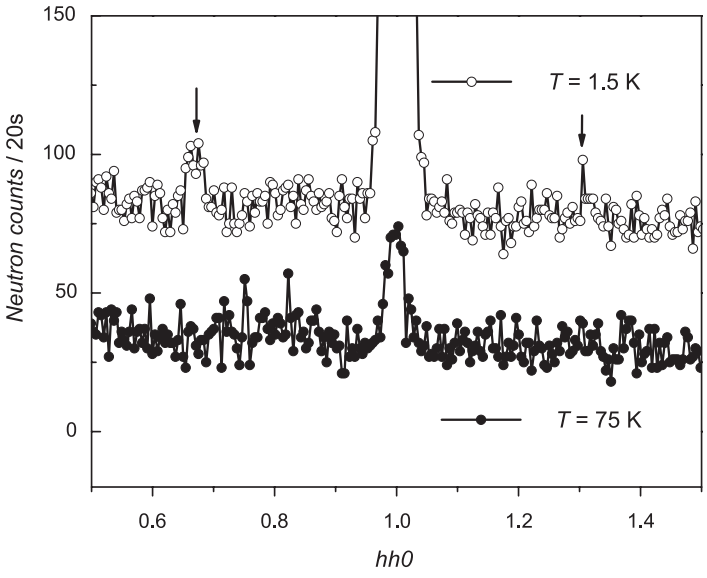

Figure 9. Neutron diffraction pattern measured along the [hh0] direction in the $\boldsymbol{a}^*$–$\boldsymbol{b}^*$ plane of the reciprocal lattice of a Tb_3Co single crystal at $T = 75$ K (full circles) and $T = 1.5$ K (open circles). The patterns are shifted from each other. The $(100)^-$ and $(100)^+$ satellite are indicated by arrows.

(110) peak and the $(110)^-$ satellite decrease with increasing temperature and approaching the critical value $T_t \approx 72$ K, while the $(000)^+$ satellite starts to grow at temperatures ∼65–68 K. This means that there is some temperature interval around $T_t \approx 72$ K in which both the low-temperature F phase and the high-temperature AF phase coexist. This is a direct evidence of

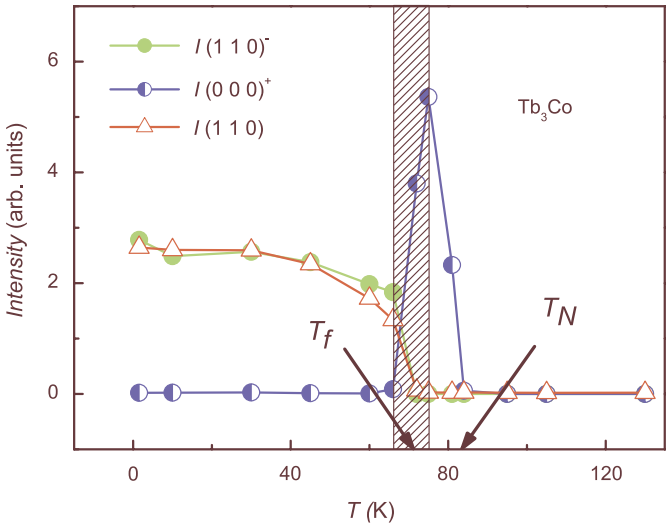

Figure 10. Temperature dependence of the intensity of the (110) Bragg reflection and satellite peaks: (0.15 0 0) and (1 1 0). The shaded area corresponds to the temperature interval where low-temperature F phase and high-temperature AF phase coexist. The intensity of the (110) reflection is divided by 50, and the intensity of the $(000)^+$ reflection is divided by 10^4.

the first-order type of the order–order transition occurring at T_t as was suggested in [16] from the specific heat measurements.

4. Conclusion

The results of the magnetic susceptibility measurements performed in the present work on single-crystalline samples of Tb_3Co have shown that this compound exhibits a significant anisotropy of the paramagnetic Curie temperatures (86, 55 and 91 K for *a*-, *b*- and *c*-axes respectively), which is associated with strong influence of the crystalline electric field. The value of the effective magnetic moment per Tb ion for Tb_3Co is found to exceed $\mu_{\rm eff} = 9.72\ \mu_{\rm B}$ for the free Tb^{3+} ion. The additional contribution $\Delta\mu_{\rm eff} \approx 0.5$–$0.9\ \mu_{\rm B}$ per Tb ion in Tb_3Co is suggested to result from spin fluctuations induced by the f–d exchange interaction in the itinerant d-electron subsystem as in other R_3T compounds [17]. The magnetization measurements in steady and pulsed magnetic fields have revealed that the Tb_3Co compound exhibits field-induced phase transitions when the field is applied along the *a*- or *b*-axes, while along the *c*-axis this compound shows a ferromagnetic-like magnetization process with a wide hysteresis loop at low temperatures. The Tb_3Co single crystal being magnetized along the *c*-axis may be characterized as a permanent magnet with the highest energy product (∼140 MG Oe at $T \sim 4$ K). The large magnetic hysteresis observed in Tb_3Co is associated apparently with an Ising-like state which starts to develop with decreasing temperature below 30 K. One may suggest that the maximal value of the coercive field in Tb_3Co is determined by exchange interactions unlike in usual high-anisotropic ferromagnetic compounds in which the hysteretic properties are controlled by the anisotropy energy. It is worth mentioning that the magnetization measurements of some liquid-quenched R_3Co alloys [33] have revealed that the hysteresis value depends on the magnetic ordering temperature, which is inherent for Ising systems. The magnetization of Tb_3Co does not show the saturation in magnetic fields up to 420 kOe along all main axes, which together with the observations of field-induced phase transitions

along the a- and b-axes is indicative of the presence of a non-coplanar magnetic structure at low temperatures. However, the values of projections of the Tb magnetic moments obtained from pulse-field measurements along main crystallographic directions are in contradiction with that derived from the commensurate model of the magnetic structure [7, 16]. Moreover, in the frame of a commensurate model, it is difficult to explain the growth of the electrical resistivity of Tb_3Co under application of the magnetic field along the a-axis [9]. According to our powder neutron diffraction measurements the incommensurate magnetic structure with $\mathbf{k} = (0.155, 0, 0)$ appears in Tb_3Co below the Néel temperature $T_N = 82$ K. This structure is found to extend at least down to ∼65 K, i.e. to a temperature lower than the critical transition temperature $T_t = 72$ K below which the magnetic structure with the ferromagnetic component along the c-axis starts to develop. Because of the coexistence of two different magnetic phases around T_t, this phase transition is identified as a first-order transition. The powder neutron diffraction patterns obtained well below T_t are found to exhibit additional magnetic reflections which cannot be described with $\mathbf{k} = (0, 0, 0)$. The NPD data are confirmed by neutron diffraction measurements on a single crystal. It has been shown that the low-temperature magnetic structure at $T < T_t$ can be described by two propagation vectors $\mathbf{k} = (0, 0, 0)$ and $\mathbf{k} = (0.32, 0.32, 0)$. One can suggest that the application of a magnetic field along the a- or b-axes of the Tb_3Co single crystal induces the phase transitions to the magnetic states with incommensurate magnetic structures having ferromagnetic components along field directions and an another periodicity in comparison with the initial zero-field magnetic structure. Such a transition may be accompanied by the positive magnetoresistance. The possibility of the appearance of incommensurate magnetic phases at low temperatures under application of a magnetic field with a longer periodicity was inferred by Gignoux and Schmitt [34] from the consideration of a mean-field model which takes into account the periodic exchange-field and crystal-field effects. Single-crystal neutron diffraction studies at various magnetic fields are needed in order to check the conjecture about the appearance of incommensurate magnetic structures in Tb_3Co above critical fields applied along the a- or b-axes. The incommensurability of the low-temperature magnetic structure, which we observed in Tb_3Co at zero fields, originates apparently from the non-Kramers character of the Tb^{3+} ion together with the exchange interaction and low-symmetry crystalline electric field. The R ion in low-symmetry sites may have a singlet ground state. In order to induce a magnetic moment on a non-Kramers ion, the exchange field acting on it has to mix the two first low-lying singlet levels forming a quasi-doublet. The existence of a quasi-doublet ground state of Tb^{3+} ions may be suggested for Tb_3Co since this compound exhibits an ordered state with large magnetic moments. It should be noted that according to specific heat measurements of Tb_3Co [17] the magnetic part of the entropy reaches at the critical temperature $T_N = 82$ K a value of about 36 J mol^{-1} K^{-1}. Since the Co ions have no magnetic moment in Tb_3Co this magnetic entropy is related to the degree of freedom of Tb angular momentum: $S_m = 3R\ln(2J + 1)$. For a Tb ion the total angular momentum J is equal to 6, and consequently the expected maximal value of $S_m = 3R\ln(13) = 63.97$ J mol^{-1} K^{-1}. The value of $S_m \approx 36$ J mol^{-1} K^{-1} $= 3R\ln(4.23)$ observed at T_N [17] is close to $3R\ln(4) = 33.7$ mol^{-1} K^{-1}, indicating that four energy levels are mainly responsible for the magnetic properties of Tb_3Co below T_N. These low-lying energy levels are apparently well separated from excited levels since the Tb_3Co compound reveals an Ising-like behaviour at low temperatures. Bearing in mind that some R_3Co compounds with Kramers R ions (R = Er [23], Dy [8] Nd [35]) exhibit complex, but *commensurate*, magnetic structures, while the Ho_3Co [13] as well as Tb_3Co (this work) compounds with non-Kramers ions show *incommensurate* structures, we suggest that the non-Kramers character of rare-earth ions is apparently a key factor which determines the incommensurability of the magnetic structure of R_3Co compounds at low temperatures.

Acknowledgments

This work was supported in part by the Swiss National Science Foundation (SCOPES 2005–2008, Project No IB7420-110849) as well as by the program of Ministry of Education and Science of the Russian Federation (Project No 2.1.1.6945). The authors are grateful to P E Markin for carrying out single-crystal orientation. Powder neutron diffraction measurements were obtained at the spallation neutron source SINQ, Paul Scherrer Institute, Switzerland. The single-crystal neutron diffraction study was carried out at the BENSC, Hahn-Meitner-Institut, Berlin, Germany.

References

[1] Gignoux D and Schmitt D 1991 *J. Magn. Magn. Mater.* **100** 99
Gignoux D and Schmitt D 1994 *J. Magn. Magn. Mater.* **129** 53
[2] Schobinger-Papamantellos P, Rodríguez-Carvaja J and Buschow K H J 2007 *J. Phys.: Condens. Matter* **19** 236201
[3] Xiao Y G, Huang Q, Ouyang Z W, Wang F W, Lynn J W, Liang J K and Rao G H 2006 *Phys. Rev.* B **73** 064413
[4] Baranov N V, Yermakov A A, Podlesnyak A, Gvasaliya S, Pirogov A N and Proshkin A V 2006 *Phys. Rev.* B **73** 104445
[5] Prokhnenko O, Kamarád J, Prokeš K, Arnold Z and Andreev A V 2005 *Phys. Rev. Lett.* **94** 107201
[6] Primavesi G J and Taylor K N R 1972 *J. Phys. F: Met. Phys.* **2** 761
[7] Gignoux D, Gomez-Sal J C and Paccard D 1982 *Solid State Commun.* **44** 695
[8] Baranov N V, Pirogov A N and Teplykh A E 1995 *J. Alloys Compounds* **226** 70
[9] Baranov N V, Markin P E, Nakotte H and Lacerda A 1998 *J. Magn. Magn. Mater.* **177–181** 1133
[10] Talik E, Mydlarz T and Gilewski A 1996 *J. Alloys Compounds* **233** 136
[11] Talik E, Witas W, Kusz J, Winiarski A, Mydlarz T, Neumann M and Böhm H 2000 *Physica* B **293** 75
[12] Baranov N V, Bauer E, Hauser R, Galatanu A, Aoki Y and Sato H 2000 *Eur. Phys. J.* B **16** 67
[13] Baranov N V, Goto T, Hilscher G, Markin P E, Michor H, Mushnikov N V, Park J-G and Yermakov A A 2005 *J. Phys.: Condens. Matter* **17** 3445
[14] Strydom O A W and Alberts L 1970 *J. Less-Common Met.* **22** 511
[15] Podlesnyak A, Daoud-Aladine A, Zaharko O, Markin P and Baranov N 2004 *J. Magn. Magn. Mater.* **272–276** 565
[16] Gignoux D and Lemaire R 1974 *ICM73: Proc. Int. Conf. on Magn (Moscow, Aug. 1973)* vol 5, p 361
[17] Baranov N V, Hilscher G, Markin P E, Michor H and Yermakov A A 2004 *J. Magn. Magn. Mater.* **272–276** 637
[18] Barbara B, Becle C, Lemaire R and Paccard D 1971 *IEEE Trans. Magn.* **7** 654
[19] Baranov N V 2004 *Phys. Met. Metallogr.* **98** (Suppl.) 10
[20] Rodríguez-Carvajal J 1993 *Physica* B **192** 55
[21] Barbara B, Becle C, Lemaire R and Paccard D 1970 *C. R. Acad. Sci. Paris* B **271** 880
[22] Gignoux D and Lemaire R 1974 *Solid State Commun.* **14** 877
[23] Baranov N V, Hilscher G, Korolev A V, Markin P E, Michor H and Yermakov A A 2002 *Physica* B **324** 179
[24] Taylor K N R and Darby M I 1972 *Physics of Rare-Earth Solids* (London: Chapman and Hall)
[25] Kirchmayr H and Poldy C A 1979 *Handbook on the Physics and Chemistry of Rare Earths* vol 2, ed K A Gschneidner Jr and L Eyring (Amsterdam: North-Holland) chapter 14
[26] Duc N H 1997 *Handbook on the Physics and Chemistry of Rare Earths* vol 24, ed K A Gschneidner Jr and L Eyring (Amsterdam: North-Holland) chapter 163
[27] Talik E and Neumann M 1994 *Physica* B **193** 207
[28] Talik E 1994 *Physica* B **193** 213
[29] Talik E, Mydlarz T, Kusz J and Böhm H 2002 *J. Alloys Compounds* **336** 29
[30] Baranov N V, Inoue K, Michor H, Hilscher G and Yermakov A A 2003 *J. Phys.: Condens. Matter* **15** 531–8
[31] Hilscher G, Michor H, Baranov N V, Markin P E and Yermakov A A 2003 *Acta Phys. Pol.* B **34** 1205
[32] Buschow K H J and van der Goot A S 1969 *J. Less-Common Met.* **18** 309
[33] Baranov N V, Pushkarski V I, Sviderski A E and Sassik H 1996 *J. Magn. Magn. Mater.* **157/158** 635
[34] Gignoux D and Schmitt D 1993 *Phys. Rev.* B **48** 12682
[35] Adachi Y, Lu Y, Umehara I, Sato K, Ohashi M, Ohoyama K and Yamaguchi Y 1999 *J. Appl. Phys.* **85** 4750